

2021-03

The characteristics of atmospheric particles and metal elements during winter in Beijing: Size distribution, source analysis, and environmental risk assessment

Zhi, M

<http://hdl.handle.net/10026.1/18240>

10.1016/j.ecoenv.2021.111937

Ecotoxicology and Environmental Safety

Elsevier BV

All content in PEARL is protected by copyright law. Author manuscripts are made available in accordance with publisher policies. Please cite only the published version using the details provided on the item record or document. In the absence of an open licence (e.g. Creative Commons), permissions for further reuse of content should be sought from the publisher or author.

1 **The characteristics of atmospheric particles and metal elements during winter in**
2 **Beijing: size distribution, source analysis, and environmental risk assessment**

3 Minkang Zhi ^a, Xi Zhang ^b, Kai Zhang ^{a*}, Simon J. Ussher ^c, Wenli Lv ^a, Yuqian Luo ^a

4 ^a State Key Laboratory of Environmental Standards and Risk Assessment, Chinese
5 Research Academy of Environmental Sciences, Beijing 100012, China

6 ^b Faculty of Environmental Engineering, The University of Kitakyushu, 1-1 Hibikino,
7 Wakamatsu, Kitakyushu, Fukuoka 808-0135, Japan

8 ^c School of Geography, Earth and Environmental Sciences, University of Plymouth,
9 Plymouth PL4 8AA, United Kingdom

10 **Abstract:** In order to investigate the pollution characteristics of size-segregated
11 particles and metal elements (MEs) after the *Chinese Air Pollution Prevention Action*
12 *Plan* was released in 2013, an intensive field campaign was conducted in the suburban
13 area of Chaoyang District, Beijing in winter 2016. The size distributions of particle
14 mass concentrations were bimodal, with the first peak in the fine fraction (0.4~2.1 μm)
15 and the second peak in the coarse fraction (3.3~5.8 μm). Moreover, the proportion of
16 fine particles increased and the proportion of coarse particles decreased as the pollution
17 level was more elevated. It was found that the composition of coarse particles is as
18 important as that of fine particles when pollution of aerosol metals in the atmosphere in
19 2016 were compared to 2013. In addition, according to the size distribution
20 characteristics, 23 MEs were divided into three groups: (a) Fe, Co, Sr, Al, Ti, Ba, and
21 U, which concentrated in coarse mode; (b) Zn, As, Cd, Tl, and Pb, which concentrated
22 in fine mode; and (c) Na, K, Be, V, Cr, Mn, Ni, Cu, Mo, Ag, and Sn, showing bimodal
23 distribution. Under clean air, slight pollution and moderate pollution conditions, most
24 elements maintained their original size distributions, while under severe pollution, the
25 unimodal distributions of most MEs became bimodal distributions. The factors analysis
26 combined with size distributions indicated that Na, Zn, Mo, Ag, Cd, and Tl, showing
27 the moderate to severe contamination on environment, were significantly influenced by
28 diffuse regional emissions or anthropogenic source emissions (vehicle exhaust
29 emissions and combustion process). The environmental risk assessment revealed that
30 the heavy metal loading in the atmospheric particles collected had a high potential for

31 ecological risk to the environment during sampling period because of the high
32 contribution of Cd, Tl, Zn and Pb.

33 **Key words:** trace metals; heavy metals; size distribution; aerosol; Enrichment factor;
34 Ecological risk; particulate matter

35 **1. Introduction**

36 In recent years, pollution of metal elements (MEs) in atmospheric particles has
37 aroused great attention because of its adverse effect on the environment (Schwartz et
38 al., 1996; Zhai et al., 2019). Airborne MEs account for a minor proportion of
39 atmospheric aerosols by mass (Bilos et al., 2001; Karaca et al., 2009; Liu et al., 2013;
40 Pancras et al., 2013), but contribute significantly to overall air pollution due to the
41 toxicity of MEs, particularly heavy metal elements, which are also non-degradable and
42 bio-enriched (Kampa and Castanas, 2008; Pacyna and Pacyna, 2001). These MEs can
43 break the balance of atmospheric environment to a large extent (Gregory et al., 1996).
44 MEs deposited to the Earth's surface also affect the aquatic and soil ecosystem (Wei et
45 al., 2019; Woszczyk et al., 2018). In addition, these effects on the ecology and
46 environment not only strongly depend on the concentrations and physico-chemical
47 properties of MEs, but also have a close association with their size distributions in
48 particles (Eleftheriadis et al., 2014; Taner et al., 2013; Yu and Huang, 2008). Some
49 previous research has shown that PM₁₀ exists in the local atmosphere and settles into
50 soil, plants and water through wet and dry deposition, which has an impact on local
51 ecosystem, whereas PM_{2.5} can exert the influence on regional ecosystem by
52 transporting far from emission sources (Hao et al., 2018; Kampa and Castanas, 2008).
53 And MEs are distributed among the wide aerodynamic size range of their constituent
54 particles (Polidori et al., 2009). Thus, the combination of concentrations and size
55 distributions of MEs is significant to assess the ecological risk assessment qualitatively
56 and quantitatively. Moreover, detailed information on the size distribution of MEs is
57 essential to identify their sources (Gao et al., 2016; Pan et al., 2015).

58 Many previous studies have investigated the size distribution of MEs in different
59 function areas (Allen et al., 2001; Silva et al., 1999; Zereini et al., 2005). The elemental

60 content of atmospheric particles is closely related to their size distribution, which is
61 directly influenced by the origin of the emissions from natural and anthropogenic
62 sources (Acosta et al., 2011; Lee et al., 2013). Li et al. (2012) found that the relatively
63 high concentrations of heavy metals were generally loaded on fine particles. Duan et al.
64 (2014) draw the conclusion that the ratios of atmospheric heavy metals such as Pb, Cd,
65 Zn, As, Cu, Cr, Ni, Mn, and V in fine particles to those in inhalable particles were from
66 46.8% to 88.5%, in accord with the research of Tan et al. (2017) and Wang et al. (2013).
67 As a result of rapid urbanization, Beijing has been a hotspot subject to anthropogenic
68 emissions of MEs (Tian et al., 2012), particularly during the heating period in autumn
69 and winter. However, the *Chinese Air Pollution Prevention Action Plan* was released in
70 2013, resulting in the removal of many sites of heavy-polluting industries from
71 Beijing. This has already shown to have had positive effects on the atmospheric
72 pollution situation (Wang et al., 2010). Hence, it is essential to analyze the size
73 distributions of atmospheric particles and MEs in Beijing under the new pollution
74 background.

75 This study presented the characteristics of 23 MEs in size-resolved aerosols
76 collected from an intensive field campaign in Beijing in winter 2016, during which the
77 air quality was highly variable. The objectives of the research were (1) to investigate
78 the size distributions of atmospheric particles and selected 23 MEs under different air
79 quality levels, (2) to identify the sources of MEs, and (3) to evaluate the environmental
80 risks of heavy metals.

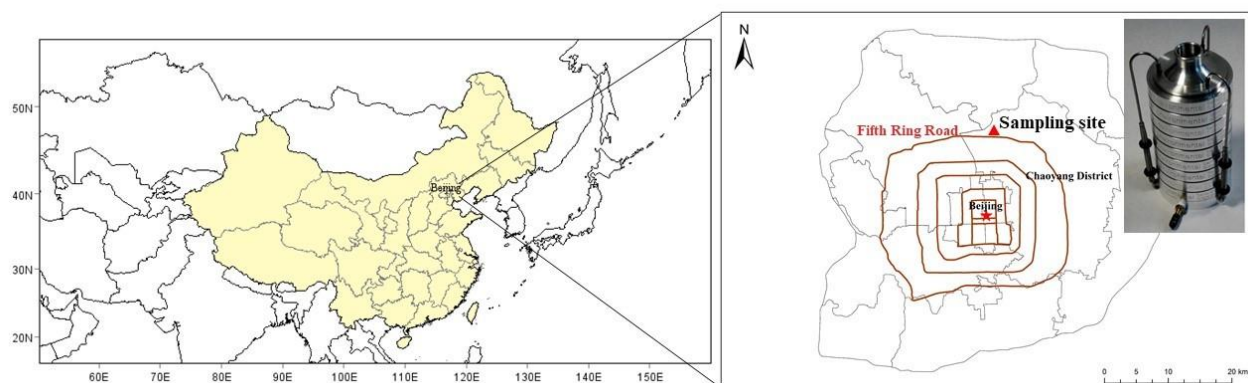
81 **2. Materials and methods**

82 **2.1 Sampling**

83 The sampling campaign of atmospheric particle collection was carried out at the
84 Chinese Research Academy of Environment Science (CRAES, 40.03°N, 116.39°E)
85 (Fig. 1). The site is located outside the 5th ring road in a suburban area of Chaoyang
86 District, Beijing with a height of 10 m. It is a mixed commercial and residential area
87 and is influenced by traffic emission, to the west is an arterial road, with a west-east
88 secondary trunk road of 100m in the south and residential buildings on both sides.

89 Otherwise, there are no other obvious nearby sources of pollution.

90 The size-resolved atmospheric particles were collected using an ambient 8-stage
91 cascade impactor sampler (Anderson Series 20-800, BGI-TISCH Inc., USA) with cut-
92 offs of 9.0, 5.8, 4.7, 3.3, 2.1, 1.1, 0.7, and 0.4 μm , operating at a flow rate of 28.3 L·min
93 $^{-1}$ in this experiment. The particle size ranges corresponding to the level of the sampler
94 and human organ in the respiratory system where the different size particles can be
95 deposited was summarized in Table 1. The sampling period was from January to March
96 2016. Each sampling lasted 48h and conducted every three times per month (the first,
97 middle and late ten days of every month). Finally, a total of 8 groups of samples were
98 obtained.



99

Fig. 1. The location of sampling site

100

101

Table 1 The particle size ranges (D_p) and human organ invaded by atmospheric particles

102

corresponding to the level of the sampler

Level	D_p (μm)	Human organ
0	>9.0	nasal cavity
1	5.8-9.0	nasal cavity
2	4.7-5.8	throat
3	3.3-4.7	bronchi
4	2.1-3.3	bronchi
5	1.1-2.1	bronchi
6	0.7-1.1	alveoli
7	0.4-0.7	alveoli

103 2.2 Elemental analysis

104 All the collected particle samples were dried for 48h and half of each filter paper
105 were put into a polytetrafluoroethylene (PTFE) digestion vial where 65% HNO₃ (3.75
106 mL), 40% H₂O₂ (1.25 mL) and 30% HF (0.20 mL) were added successively. Then the
107 solutions were heated by the oven (Yamato), with the temperature and duration of
108 185 °C and 8h, respectively. After the heating process, the digested particles samples
109 were diluted with distilled water constant volume to 15 mL. Finally, 6 mL of the sample
110 solution was taken out and the concentrations of MEs were measured by ICP-OES
111 (iCAP™ 7000 Series, Thermo Scientific™, MA, USA) and ICP-MS (Agilent
112 Technologies, Tokyo, Japan), simultaneously. In addition, internal standards (⁸⁹Y, ¹⁹³Ir,
113 ¹¹⁵In and ¹⁰³Rh) were added online during MEs analysis (Pan and Wang, 2015).

114 2.3 Quality assurance (QA) and quality control (QC)

115 The pre-treatment and analytical procedure of samples followed a strict QA/QC
116 process. The replicate field blanks and filter samples were handled identically to assess
117 the error during both sampling and data processing (Pekney and Davidson, 2005). In
118 order to assess the validity of data and select a group of reliable data obtained by two
119 instruments, the limits of detection (LODs) were calculated as three times the standard
120 deviation (SD) for the blank samples. All results are listed in Table 2. which also
121 shows the calculated mean and SD of ME concentration in the filter samples. For the
122 two analytic techniques of ICP-OES and ICP-MS, the average concentrations and SD
123 of MEs in the size-resolved particles were calculated separately then summarized in the
124 supplement table and to prevent misuse of the data below the LODs of these instruments,
125 they were listed as <b.d.l. and omitted in the data processing. The average
126 concentrations of blanks samples were well below that of filter samples and MEs'
127 concentrations in the filter samples were above LODs so that blank samples did not
128 exert an important influence on the observed concentrations. However, the average
129 concentrations of As, Se and Pb of filter samples were below that of blank samples and
130 the concentrations of Mg, Al and Ca in the field blanks were below the LODs of

131 instrument, which were analyzed by ICP-OES. In addition, Fe and Zn, abundant in the
 132 environment, could be measured more accurately by ICP-OES (Cruz et al., 2015). So
 133 the concentrations of Na, K, Fe and Zn used the data of ICP-OES, while that of other
 134 MEs chose from ICP-MS.

135 Additionally, reference materials of fly ash (GBW08401) and soil (GBW07401)
 136 were acid digested and measured in parallel with the filters samples to measure the
 137 recoveries (Pan et al., 2015). The recoveries of MEs are within the target recoveries
 138 ($100 \pm 15\%$), with the exception of Se. Thus, this study only presents 23 MEs (As, Fe,
 139 Pb, Cd, Ni, Cu, Zn, Cr, Ti, Al, K, Na, Mn, V, Ba, Tl, Be, Co, Sr, Mo, Ag, Sn, U).

140 Table 2. Field blanks and limit of detection of the MEs subject to microwave digestion with
 141 $\text{HNO}_3/\text{H}_2\text{O}_2/\text{HF}$.

Elements	ICP-OES		ICP-MS	
	Air ($\text{ng}\cdot\text{m}^{-3}$) ^a	Limit of detection ($\text{ng}\cdot\text{m}^{-3}$) ^c	Air ($\text{ng}\cdot\text{m}^{-3}$) ^b	Limit of detection ($\text{ng}\cdot\text{m}^{-3}$) ^d
Na	85.04	56.32		
Mg	-1.40	1.95		
Al	-0.87	3.36	0.815	0.919
K	16.53	23.88		
Ca	-2.85	1.19		
V	-0.20	6.24	0.003	0.008
Cr	0.38	8.73	0.027	0.100
Mn	0.07	1.60	0.012	0.013
Fe	0.75	4.27	0.175	0.299
Ni	-2.87	10.46	0.010	0.008
Cu	-1.94	2.69	0.048	0.082
Zn	1.04	3.18	0.131	0.142
As	83.51	84.05	0.004	0.006
Se	60.44	76.98	0.005	0.010
Mo			0.015	0.034
Cd	1.47	4.61	0.002	0.001
Ba	0.09	0.21	0.009	0.032
Pb	38.11	66.65	0.044	0.172
Ti	-1.90	3.75	0.037	0.144
Tl	-58.57	63.69	0.001	0.001
Be	-0.63	0.71	0.000	0.000
Co			0.002	0.004
Sr			0.049	0.011
Ag			0.031	0.019

Sn	0.039	0.109
Sb	0.023	0.070
U	0.001	0.002

142 Note: ^a and ^b: Field blanks in air were respectively calculated to be equal to mean values of element
 143 mass concentrations in six filter blanks used by the ICP-OES and ICP-MS;
 144 ^c and ^d: Limit of detection (LOD) corresponding to three times the standard deviation of the six
 145 blank signals obtained by using the ICP-OES and ICP-MS respectively.

146 2.4 Data analysis

147 2.4.1 Enrichment factor

148 To evaluate the contamination level of metal elements, the crustal enrichment
 149 factors (EFs) were calculated as follows (Luo et al., 2015):

$$150 \quad EF = \frac{(C_i/C_R)_{sample}}{(C_i/C_R)_{background}} \quad (1)$$

151 where, C_i and C_R are the concentrations of selected MEs and reference element in
 152 sample and background crust (Cheng et al., 2014), respectively. Aluminum served as
 153 the reference element in this study. This method facilitates the determination of the
 154 source contribution of MEs originated from natural and anthropogenic emissions (Wang
 155 et al., 2018). In general, $EF \leq 1$ indicates that MEs are mainly from natural sources such
 156 as road dust, while $EF > 1$ is deemed to be from anthropogenic sources. The larger the
 157 value of EF, the higher the degree of enrichment of MEs.

158 2.4.2 The geo-accumulation index

159 The geo-accumulation index (I_{geo}) is introduced to draw a comparison between the
 160 background levels and concentrations of MEs in particles to analysis local pollution
 161 levels of MEs (Censi et al., 2017; Li et al., 2015), calculated by Eq. (2) (Müller, 1969):

$$162 \quad I_{geo} = \log_2 \frac{(C_i)_{sample}}{1.5 \times (C_i)_{background}} \quad (2)$$

163 where, the meanings of C_i are equal to that of EF and same data are used to calculate it.
 164 The factor 1.5 is applied as the background matrix correction value. The pollution levels
 165 of MEs at sampling site are divided into seven categories according to the values of I_{geo} :
 166 uncontaminated ($I_{geo} \leq 0$), slightly contaminated ($0 < I_{geo} \leq 1$), moderately contaminated
 167 ($1 < I_{geo} \leq 2$), moderately to strongly contaminated ($2 < I_{geo} \leq 3$), strongly contaminated

168 ($3 < I_{\text{geo}} \leq 4$), strongly to severely contaminated ($4 < I_{\text{geo}} \leq 5$), and severely contaminated
169 ($I_{\text{geo}} > 5$) (Wei et al., 2015).

170 2.4.3 The potential ecological risk index

171 This study used the potential ecological risk index proposed by Hakanson (1980)
172 to evaluate the environmental influence of heavy metal elements in particles. The
173 method builds up a bond between the environmental ecological effect and toxicological
174 characteristics of heavy metals, comprehensively assessing the potential risk of heavy
175 metals in environment. The potential ecological risk index of a single element (E_r^i) and
176 comprehensive potential ecological risk index (RI) can be calculated by using the
177 following equations:

$$178 \quad C_f^i = (C_i)_{\text{sample}} / (C_i)_{\text{background}} \quad (3)$$

$$179 \quad E_r^i = T_r^i \times C_f^i \quad (4)$$

$$180 \quad RI = \sum E_r^i \quad (5)$$

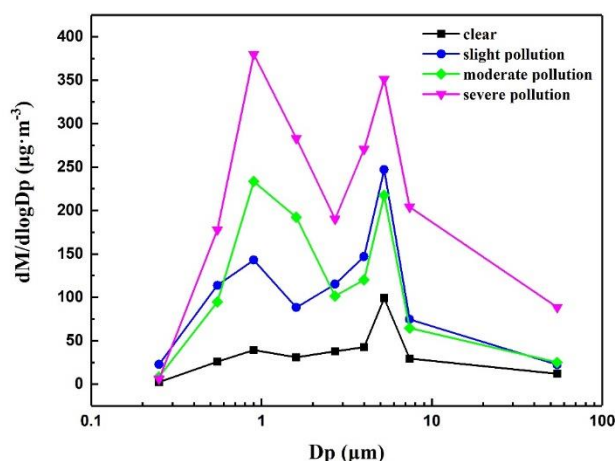
181 where, the meanings of C_i are equal to that of EF and I_{geo} , C_f^i is the contamination factor
182 of the metal i and T_r^i is the toxic-response factor of the metal i , which is determined
183 for Ti=Mn=Zn=1, V=Cr=2, Cu=Ni=Co=Pb=5, Tl=As=10 and Cd=30 according to
184 previous studies (Douay et al., 2013; Egbueri, 2020; Liu et al., 2018). Due to little
185 toxicological effects for mineral elements and absence of T_r^i of some elements, the
186 potential ecological risks of only 12 elements (Zn, Co, V, Cr, Mn, Ti, Ni, Cu, As, Cd,
187 Tl and Pb) were analyzed in this study. On the basis of its severity, the ecological risks
188 were divided into five levels: slight risk ($E_r^i < 40$); moderate risk ($40 < E_r^i < 80$); strong
189 risk ($80 < E_r^i < 160$); very strong risk ($160 < E_r^i < 320$); extremely strong risk ($E_r^i > 320$).
190 Similarly, the scopes of RI were ~ 150 , $150 \sim 300$, $300 \sim 600$ and $600 \sim$ for low ecological
191 risk, moderate ecological risk, high ecological risk and very high ecological risk (Gujre
192 et al., 2021; Williams and Antoine, 2020).

193 3. Results and discussion

194 3.1 Particle mass concentration

195 The air quality is classified into four levels: clear ($PM_{2.1} \leq 50 \mu\text{g}\cdot\text{m}^{-3}$), slight

196 pollution ($50 < \text{PM}_{2.1} \leq 100 \mu\text{g}\cdot\text{m}^{-3}$), moderate pollution ($100 < \text{PM}_{2.1} \leq 150 \mu\text{g}\cdot\text{m}^{-3}$), and
197 severe pollution ($\text{PM}_{2.1} > 150 \mu\text{g}\cdot\text{m}^{-3}$). The average mass concentrations of $\text{PM}_{2.1}$ in
198 Beijing were $24.16 \mu\text{g}\cdot\text{m}^{-3}$, $94.34 \mu\text{g}\cdot\text{m}^{-3}$, $127.88 \mu\text{g}\cdot\text{m}^{-3}$, $200.89 \mu\text{g}\cdot\text{m}^{-3}$ in four levels,
199 respectively. Fig. 2 showed that the size distributions of particle mass concentrations
200 were all bimodal in four levels. The first peak was in the fine fraction ($0.4\sim 2.1 \mu\text{m}$) and
201 the second peak occurred in the coarse fraction ($3.3\sim 5.8 \mu\text{m}$). Atmospheric particles in
202 the coarse fraction were accumulated in all aerosol conditions including clear and slight
203 pollution, accounting for 30.98% and 25.36% of total mass concentration, respectively.
204 However, the atmospheric particles in fine fraction had relatively larger contributions
205 under moderate pollution and severe pollution (22.08% and 20.55%) compared to that
206 in coarse fraction (19.46% and 18.01%). These observations revealed that as the
207 pollution level intensified, the concentrations of fine particles, especially at the size
208 range of $0.4\sim 2.1 \mu\text{m}$, increased, which was the main cause of the deterioration of air
209 quality in Beijing. In comparison, the average mass concentration of fine particles in
210 2013 prior to air quality legislation ranged from 148.69 to $180.00 \mu\text{g}\cdot\text{m}^{-3}$, which was
211 higher than that of our result ($111.80 \mu\text{g}\cdot\text{m}^{-3}$). Moreover the size distribution of particle
212 mass concentrations was centered at $D_p \leq 1.0 \mu\text{m}$, accounting for approximately
213 63.50~72.70% of total concentration (Wang et al., 2014; Zhu et al., 2016). It is showed
214 that the main constituents of atmospheric particles were fine particles in Beijing in 2013.
215 In addition, Shao et al. (2018) also observed the downward trend of annual fine
216 particles concentration from 2013 to 2016 in Beijing. These phenomena revealed the
217 important effect of the *Chinese Air Pollution Prevention Action Plan* released in 2013,
218 alleviating the atmospheric pollution situation in Beijing obviously and manifesting the
219 size distribution as the coarse fraction was as important as the fine fraction in particles
220 in Beijing.



221

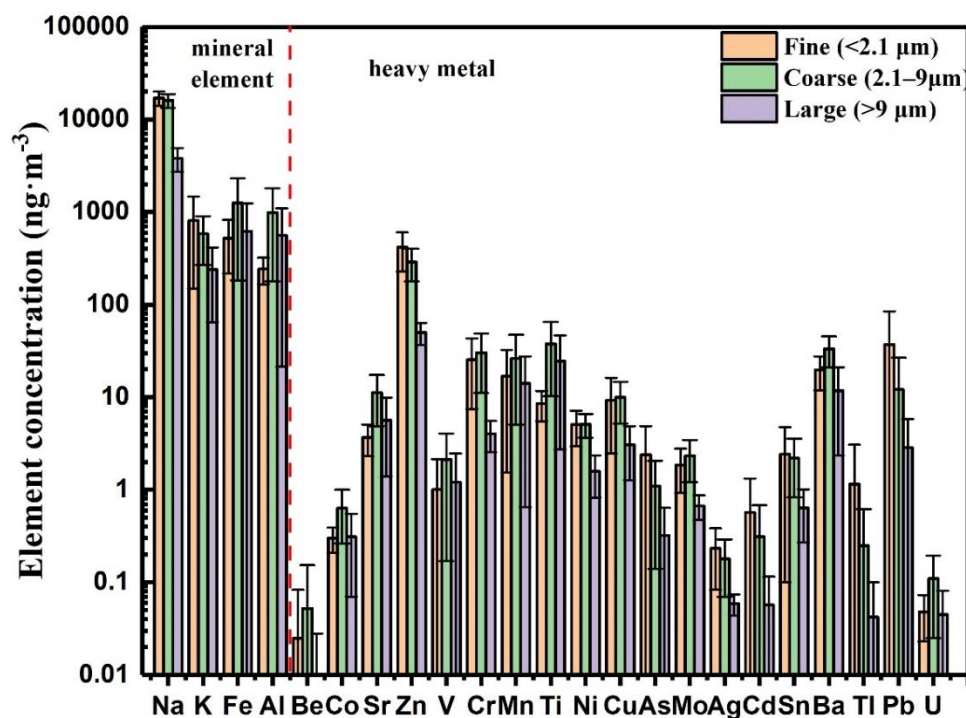
222 Fig. 2. Size distributions of particle mass concentration in different air quality levels

223 3.2 Element concentration and size distribution

224 3.2.1 Elemental concentrations in size-resolved particles

225 Atmospheric particles with high loading of MEs will cause adverse effects on the
 226 environment and human health. Based on the cut points of the sampler, the atmospheric
 227 particles were further divided into fine mode (<2.1 µm), coarse mode (2.1-9.0 µm), and
 228 large mode (>9.0 µm). As shown in Fig. 3, the atmospheric MEs generally accumulated
 229 more in the fine and coarse mode particles than that in large mode particles, with the
 230 average concentrations of 19.22, 19.31, and 5.36 µg·m⁻³, respectively, which was
 231 consisted with previous research (Pan et al., 2013; Zhang et al., 2019). This suggests
 232 that smaller particles with higher specific surface areas have more active sites around
 233 the surfaces and stronger adsorption in the fine and coarse mode, compared with large
 234 mode particles.

235 MEs can be divided into mineral elements (Na, Fe, Al, K) and heavy metal
 236 elements (other 19 elements). The average concentrations of mineral elements were 2~5
 237 orders of magnitude higher than heavy metals in samples. The contents of Na were all
 238 the highest among the mineral elements in three mode particles, followed by Fe, Al, K.
 239 Moreover, the mineral elements tended to be enriched in the particles with size range
 240 lower than 9.0 µm. For heavy metals, Zn was the most abundant element, followed by
 241 Ti, Mn, Cr, Ba, and Pb, while other heavy metals accounted for a relatively small
 242 proportion by mass in particles.



243

244

Fig. 3. Mass concentrations of metal elements in size-resolved particles

245

3.2.2 Size distribution

246

According to the similarities of the size distributions, 23 MEs were clarified into three groups.

248

The first group included Fe, Co, Sr, Al, Ti, Ba, and U, which were abundant in coarse mode with the majority of the mass centered at 4.7 μm and 5.8 μm (Fig. 4(a)), indicating that they mainly originated from natural sources, e.g., coarse particles produced by mechanical processes (Kandler et al., 2009). These elements in the coarse fraction (3.3~5.8 μm) accounted for 52.31% (U)~71.37% (Ti), in contract, these elements in large model particles were ultra-low with the percentage of only 5.01% of the total concentration. Considering the location of the sampling site, it can be inferred that the main source of these elements was the road dust caused by soil suspension and accumulated wind-blown dust, not anthropogenic emission (Gao et al., 2014; Ji et al., 2016). In addition, the size distributions of Co, Sr, Al, Ti, Ba, U varied from unimodal to bimodal distribution from clear to severe pollution (Supplement figure), which is most likely caused by the vehicle exhaust emission and regional transmission in Beijing

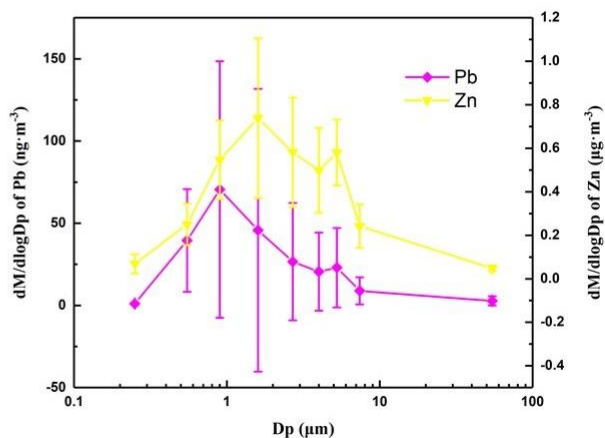
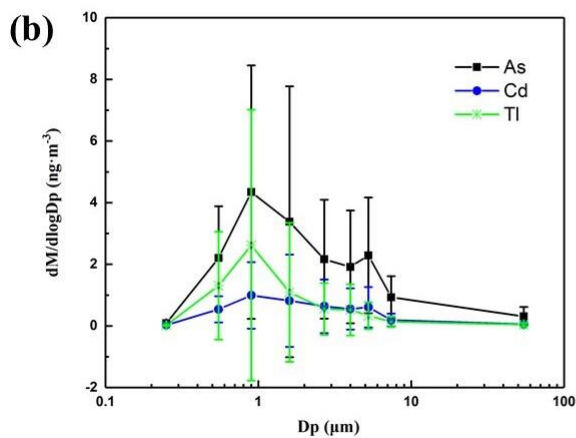
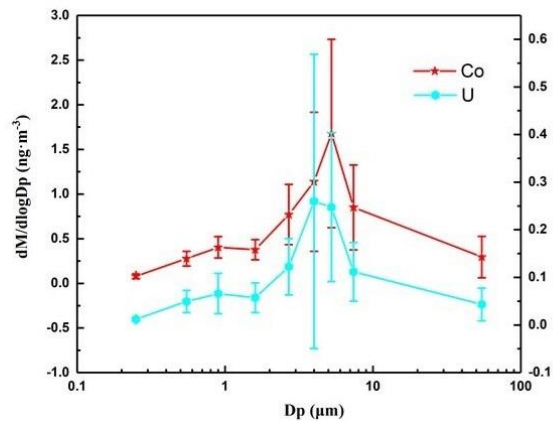
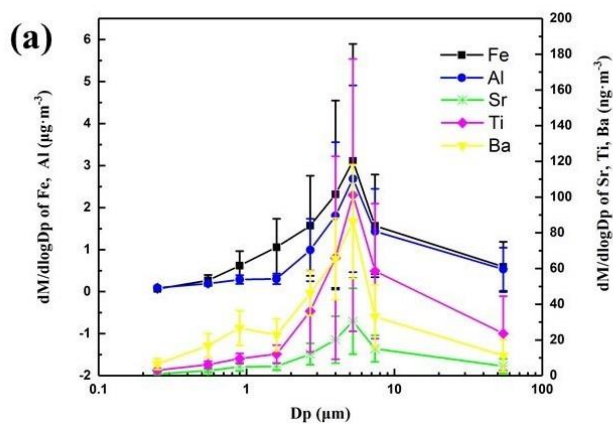
259

260 (Pan et al., 2013; Tong et al., 2020).

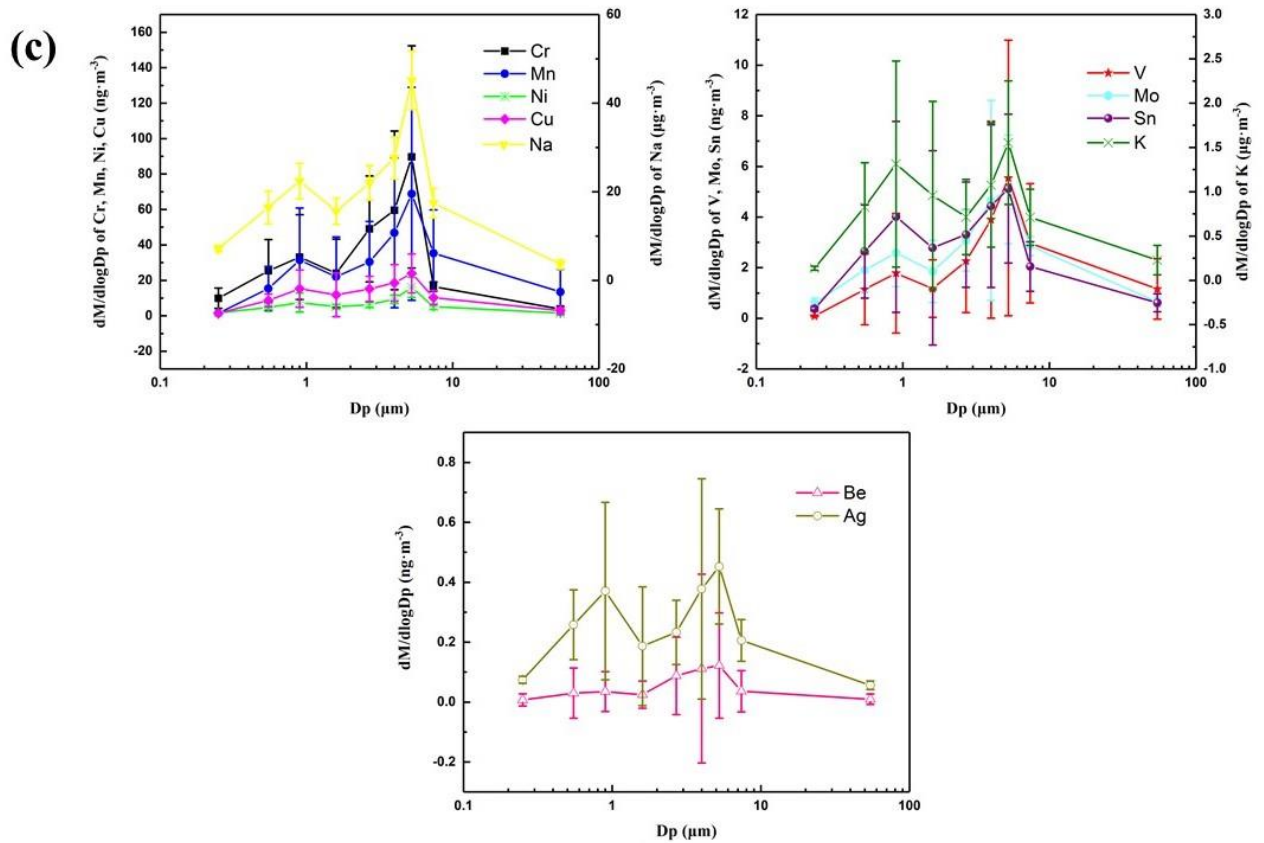
261 The second group consisted of Zn, As, Cd, Tl, and Pb, and these elements only had
262 a peak in the fine mode (Fig. 4(b)), which suggested the effect of anthropogenic sources.
263 Among these five elements, As, Cd, Tl, and Pb had a peak in the fine fraction (0.4~2.1
264 μm), and their percentages ranged from 53.22% (Cd) to 75.79% (Tl) of the total
265 concentrations. In addition, these four elements all turned into bimodal distribution
266 under moderate and severe pollution and showed an additional minor peak at 4.7~5.8
267 μm (Supplement figure). Linak et al. (2000) showed that As, Pb and Cd from
268 incineration chambers had similar bimodal particle size distribution. Hence, these MEs
269 were mainly caused by coal combustion during the heating period in winter. As for Zn,
270 its concentration was concentrated in a wide particle size range from 0.7 to 5.8 μm , and
271 the contribution concentration at 0.7~2.1 μm occupied about 52.54% of the total
272 concentration, mainly causing by vehicle emissions and road dust (Chen et al., 2010).
273 Moreover, the average concentration of Zn in our clear pollution level ($0.41 \mu\text{g}\cdot\text{m}^{-3}$)
274 was higher than that of slight pollution ($0.31 \mu\text{g}\cdot\text{m}^{-3}$), and the average concentration in
275 moderate pollution ($0.59 \mu\text{g}\cdot\text{m}^{-3}$) was similar to that of severe pollution ($0.56 \mu\text{g}\cdot\text{m}^{-3}$),
276 indicating that the content of Zn had no positive correlation with air pollution level and
277 the effect of natural sources was as significant as that of anthropogenic activities.

278 The third group including Na, K, Be, V, Cr, Mn, Ni, Cu, Mo, Ag and Sn, presented
279 a bimodal distribution, with the first peak at fine mode (0.4~2.1 μm) and the second
280 peak at coarse mode (3.3~5.8 μm) (Fig. 4(c)), in line with multiple sources, i.e., natural
281 and anthropogenic emissions. These elements in the fine mode accounted for 19.29%
282 (Be) to 41.21% (K) of the total concentration and 44.44% (K) to 61.98% (V) in coarse
283 mode. The elemental concentrations were all relatively high in two fractions, but more
284 centralized in the coarse mode, indicating that these elements mainly caused by road
285 dust. In addition, the size distributions of V, Cr and Mn were unimodal structure with a
286 peak at coarse mode under clear and slight pollution (Supplement figure). Be and Ni
287 showed various distribution forms under four levels, but more accumulated in the
288 coarse mode particles, particularly in moderate and severe pollution, manifesting that
289 these elements were rarely affected by the anthropogenic sources. As the pollution

290 levels aggravated, the loading concentration of K within submicron particles smaller
 291 than 0.7 μm was increased, which may be attributable to biomass burning (Li et al.,
 292 2014; Silva et al., 1999).



294



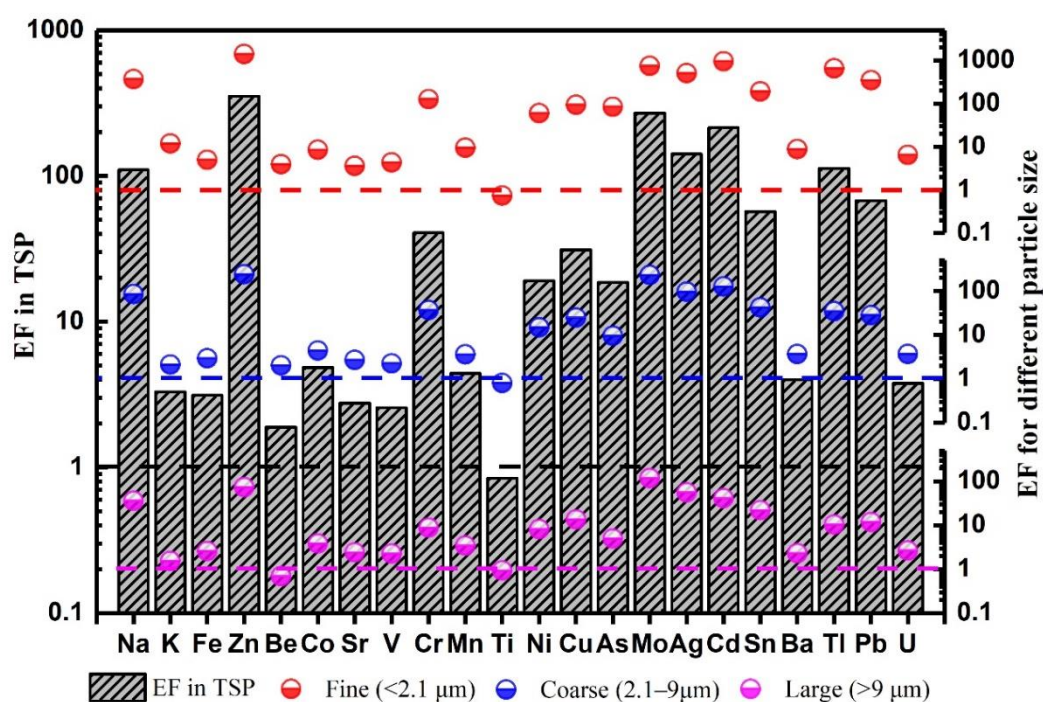
295

296 Fig. 4. The size distributions of selected 23 metal elements in particles during the Beijing winter
 297 (unimodal in coarse mode (a), unimodal in fine mode (b), and bimodal (c)). The data point is the
 298 average concentration of metal elements during eight sampling periods and the error bar is SD.

299 3.3 Source determined by enrichment factor

300 Enrichment factor (EF) was employed to evaluate the contamination level and
 301 differentiate the source contribution of MEs originated from natural and anthropogenic
 302 emissions. Fig. 5 showed the average enrichment of MEs in different mode particles.
 303 For TSP, the EF value of Ti was less than 1, which was from natural sources. Other MEs
 304 in TSP could be divided into three groups according to their EFs values. The values of
 305 EFs for K, Fe, Be, Co, Sr, V, Mn, Ba and U were relatively low (<10), particularly in
 306 the large mode particles, suggesting that these elements, slight degree of enrichment,
 307 mainly originated from re-suspended soil (Polidori et al., 2009). Cr, Ni, Cu, As, Sn, Pb
 308 showed the intermediately enriched group with EFs between 10 and 100. And other six
 309 elements (Na, Zn, Mo, Ag, Cd, and Tl) were dominated by anthropogenic sources
 310 (vehicle exhaust emissions and combustion process) (Huang et al., 1994), and the

311 highly enriched group with the EFs higher than 100. Moreover, Zn, Mo and Cd had the
 312 highest EFs in each size fraction (EF exceed or was approximately equal to 100),
 313 indicating that the worst-affected elements were Zn, Mo and Cd of selected 23 MEs by
 314 anthropogenic sources. The elements of Cr, Ag, Tl, Sn and Pb also became high
 315 enrichment degree in fine mode particles, moreover, the EF of Zn even exceeded 1000.
 316 So these heavy metals were mainly influenced by anthropogenic emissions. In addition,
 317 Na was a mineral element, while its EF values in large, coarse and fine particles were
 318 relatively high (36.49, 86.39 and 374.61). Oetari et al. (2019) and Meij and te Winkel
 319 (2007) have confirmed that the content of Na in atmospheric particles had strong
 320 relationship with coal combustion. Hence, in this study, the high enrichment of Na was
 321 likely derived from combustion sources during the heating period in winter combined
 322 with the sampling site, locating on the rural-urban fringe zone. The comparison of the
 323 EFs for each element among 3 different size fraction showed that the enrichment levels
 324 of elements increased as particle size decreased, which was consisted with previous
 325 researches (Pan et al., 2013; Pancras et al., 2013), revealing the significant environment
 326 effect of fine particles.



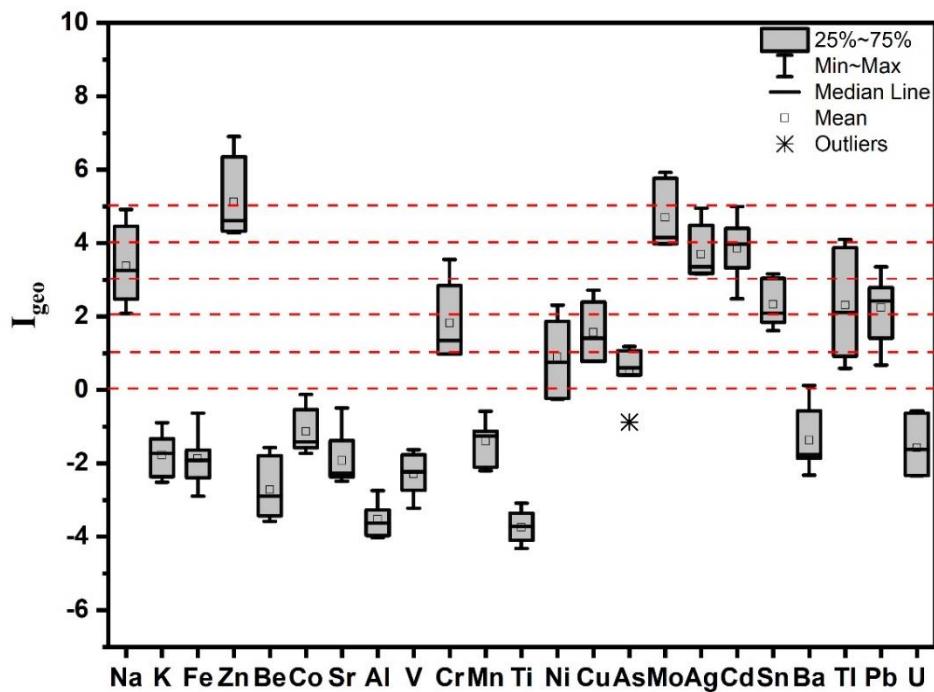
328 Fig. 5. Enrichment factors (EFs) of metal elements in TSP, fine mode, coarse mode, and large
329 mode particles in Beijing. EF=1 in TSP and different size-resolved particles was marked by the
330 dash line, colored by corresponding color.

331 3.4 Environmental risk assessment

332 To evaluate the overall environmental pollution degree and ecological risk in
333 Beijing, the concentrations of MEs in TSP, obtained by adding the average
334 concentrations of 9 size ranges, were used to calculate I_{geo} and the potential ecological
335 risk index. As shown in Fig. 6, the I_{geo} values of K, Fe, Be, Co, Sr, Al, V, Mn, Ti, Ba
336 and U were less than 0, indicating that these MEs can not cause environment
337 contamination. Moreover, these elements of $I_{geo} < 0$ displayed no or low degree of
338 enrichment combined with the values of EFs. It was confirmed that the effect of MEs
339 originated from anthropogenic emissions was more significant than that from natural
340 sources on the environment. The average I_{geo} values of Ni and As were smaller than 1,
341 and that of Na, Cr, Cu, Ag, Cd, Sn, Tl and Pb were between 1 and 4, which revealed
342 slight contamination by Ni and As, and moderate to strong contamination by Na, Cr,
343 Cu, Ag, Cd, Sn, Tl and Pb. However, 25.00% of the sampling periods belonged to
344 strongly to severely contaminated categories for Na, Ag and Cd ($4 \leq I_{geo} \leq 5$). The I_{geo}
345 values of Zn and Mo were the highest of all MEs with main ranges of I_{geo} (Zn) > 5 and
346 $4 \leq I_{geo}$ (Mo) ≤ 5 ; thus these two elements could cause serious pollution for the
347 environment.

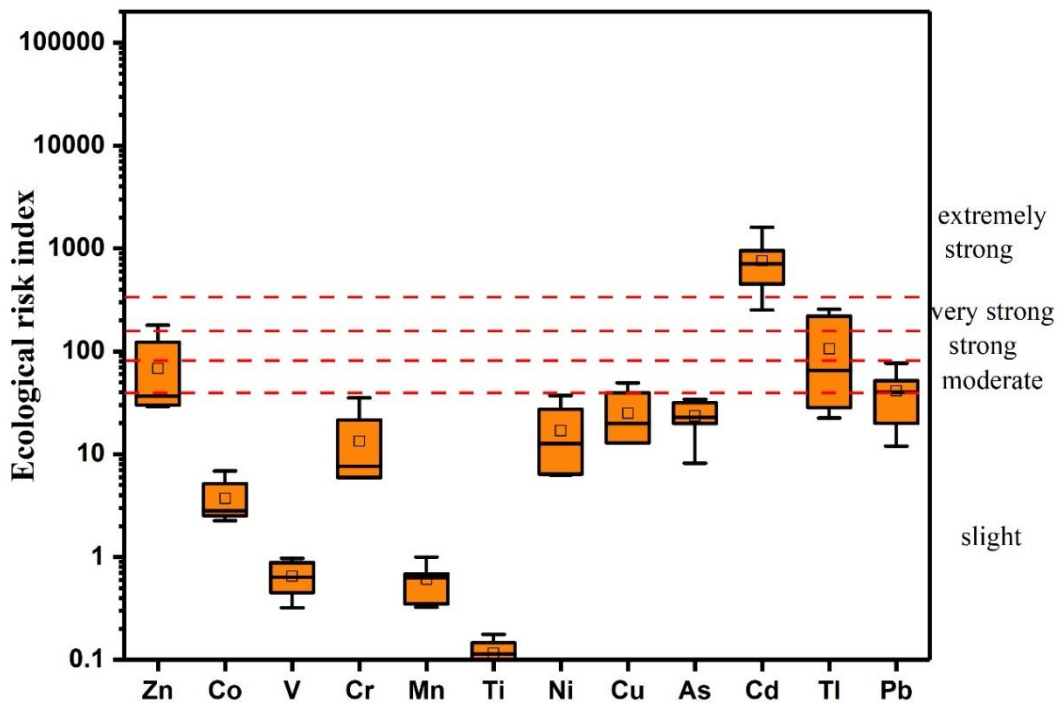
348 Fig. 7 indicated the potential ecological risk index of 12 heavy metals, and the
349 comprehensive potential ecological risk index (RI) was calculated during the sampling
350 period. The values of RI ranged from 363.97 to 2054.02 with a mean value of 926.87,
351 demonstrating that the atmospheric particles showed the high potential ecological risk
352 during winter time in Beijing. To be specific, Cd, Tl, Zn, and Pb were the most
353 important pollution elements for the environment, with the E_r^i values of 759.97, 105.91,
354 67.95, and 41.20, respectively. Hence, it is significant to identify the sources of these
355 four elements and decrease their emission amounts, especially Cd. The comparatively
356 higher ecological risks posed by Cd and Cu in the road dust of industrial areas have

357 been attributed to smelting and ironworks, and electronic wastes from factories, but not
358 existed in Beijing (Shahab et al., 2020). Therefore, we can infer that atmospheric
359 particles contained Cd may come from regional transmissions of peripheral steel
360 smelting plants, be deposited onto road, thereby exerting adverse potential ecological
361 risk on environment.



362

363 Fig. 6. The geo-accumulation index (I_{geo}) of elements from January to March 2016 in Beijing



364

365

Fig. 7. The potential ecological risk of heavy metals in atmospheric particles

366

The ecological risks of 12 heavy metals were divided into five levels according to the values of E_r^i , as described above and the corresponding level limits were marked by red dash line in the figure.

367

368 4. Conclusions

369

The size-resolved atmospheric particulate samples in Beijing were collected to analyze the size distributions of particle mass concentrations and selected 23 MEs during January to March 2016. Combined with the EF analysis and other model parameters, the intensive data analysis campaigns investigated the source of MEs in particles and evaluated their environmental risks. The results lead to the following conclusions.

374

375

- (1). The size distributions of particle mass concentrations all were bimodal in four air quality levels, i.e., the first at fine fraction (0.4~2.1 μm) and the second at coarse fraction (3.3~5.8 μm). The atmospheric particles were accumulated easily in coarse fraction in clear and slight pollution. But under moderate and severe pollution, the proportion of particles in the fine fraction increased and in the coarse mode decreased, showing the significant emissions of fine

380

381 particles in Beijing, in accord with the comparison of the EFs among 3
382 different size fractions.

383 (2). According to the similarities of the size distributions, 23 MEs are divided into
384 three groups: (a) elements (Fe, Co, Sr, Al, Ti, Ba, U) showing the unimodal
385 distribution, which were abundant in coarse mode; (b) elements (Zn, As, Cd,
386 Tl, Pb) showing unimodal structure with a peak in fine mode particles; (c)
387 elements (Na, K, Be, V, Cr, Mn, Ni, Cu, Mo, Ag, Sn) with a bimodal
388 distribution throughout the size range (centered at approximately 0.55~1.60
389 μm and 4.00~7.40 μm). The size distributions of MEs in four air quality levels
390 varied greatly. For the MEs of unimodal distribution, most elements
391 maintained their original size distributions under clear and slight pollution,
392 while in the case of severe pollution, showing the bimodal distribution, except
393 for Fe and Zn. These findings suggest that the composition of coarse particles
394 is as important as that of fine particles to alleviate heavy metal pollution in the
395 modern urban atmosphere.

396 (3). The source emission and environmental risk varied with the elemental
397 composition of atmospheric particles and were identified by the factor analysis
398 applied on the elemental data combined with the size distributions. Na, Zn, Mo,
399 Ag, Cd, and Tl showed high enrichment degrees and moderate to severe
400 contamination on the environment, signifying influences from regional
401 transmissions or anthropogenic emissions, e.g., vehicle exhaust emissions and
402 coal combustion. Other elements may originate from multiple sources, i.e.,
403 anthropogenic emissions and road dust, except for Ti. In addition, Beijing's
404 atmospheric particles showed the high potential ecological risk in winter
405 according to the values of RI. To be specific, Cd, Tl, Zn, and Pb were the most
406 important pollution elements for the environment, with the E_T^i values of 759.97,
407 105.91, 67.95, and 41.20, respectively. Hence, the pollution of metal elements
408 should cause concern for people, especially Cd.

409 **Acknowledgments**

410 Funding: This work was supported by the National Research Program for Key
411 Issues in Air Pollution Control (No.DQGG0304-05) and the Fundamental Research
412 Funds for Central Public Welfare Scientific Research Institute of China
413 (No.2016YSKY-025). The European Commission Marie Skłodowska Curie Career
414 Integration Grant supported time and resource for SJU (PCIG-GA-2012-778 333143
415 ‘DISCOSAT’).
416

- 418 Acosta, J.A., Faz, Á., Kalbitz, K., Jansen, B., Martínez-Martínez, S., 2011. Heavy metal concentrations
419 in particle size fractions from street dust of Murcia (Spain) as the basis for risk assessment. *J.*
420 *Environ. Monit.* 13, 3087–3096. <https://doi.org/10.1039/c1em10364d>
- 421 Allen, A.G., Nemitz, E., Shi, J.P., Harrison, R.M., Greenwood, J.C., 2001. Size distributions of trace
422 metals in atmospheric aerosols in the United Kingdom. *Atmos. Environ.* 35, 4581–4591.
423 [https://doi.org/10.1016/S1352-2310\(01\)00190-X](https://doi.org/10.1016/S1352-2310(01)00190-X)
- 424 Bilos, C., Colombo, J.C., Skorupka, C.N., Rodriguez Presa, M.J., 2001. Sources, distribution and
425 variability of airborne trace metals in La Plata City area, Argentina. *Environ. Pollut.* 111, 149–158.
426 [https://doi.org/10.1016/S0269-7491\(99\)00328-0](https://doi.org/10.1016/S0269-7491(99)00328-0)
- 427 Censi, P., Cibella, F., Falcone, E.E., Cuttitta, G., Saiano, F., Inguaggiato, C., Latteo, V., 2017. Rare earths
428 and trace elements contents in leaves: A new indicator of the composition of atmospheric dust.
429 *Chemosphere* 169, 342–350. <https://doi.org/10.1016/j.chemosphere.2016.11.085>
- 430 Chen, X., Xia, X., Zhao, Y., Zhang, P., 2010. Heavy metal concentrations in roadside soils and
431 correlation with urban traffic in Beijing, China. *J. Hazard. Mater.* 181, 640–646.
432 <https://doi.org/10.1016/j.jhazmat.2010.05.060>
- 433 Cheng, H., Li, K., Li, M., Yang, K., Liu, F., Cheng, X., 2014. Geochemical background and baseline
434 value of chemical elements in urban soil in China. *Earth Sci. Front.* 21, 265–306.
435 <https://doi.org/10.13745/j.esf.2014.03.028>
- 436 Cruz, S.M., Schmidt, L., Dalla Nora, F.M., Pedrotti, M.F., Bizzi, C.A., Barin, J.S., Flores, E.M.M., 2015.
437 Microwave-induced combustion method for the determination of trace and ultratrace element
438 impurities in graphite samples by ICP-OES and ICP-MS. *Microchem. J.* 123, 28–32.
439 <https://doi.org/10.1016/j.microc.2015.05.008>
- 440 Douay, F., Pelfrène, A., Planque, J., Fourrier, H., Richard, A., Roussel, H., Girondelot, B., 2013.
441 Assessment of potential health risk for inhabitants living near a former lead smelter. Part 1: Metal
442 concentrations in soils, agricultural crops, and homegrown vegetables. *Environ. Monit. Assess.* 185,
443 3665–3680. <https://doi.org/10.1007/s10661-012-2818-3>
- 444 Duan, J., Tan, J., Hao, J., Chai, F., 2014. Size distribution, characteristics and sources of heavy metals in
445 haze episod in Beijing. *J. Environ. Sci. (China)* 26, 189–196. [https://doi.org/10.1016/S1001-0742\(13\)60397-6](https://doi.org/10.1016/S1001-0742(13)60397-6)
- 447 Egbueri, J.C., 2020. Groundwater quality assessment using pollution index of groundwater (PIG),
448 ecological risk index (ERI) and hierarchical cluster analysis (HCA): A case study. *Groundw.*
449 *Sustain. Dev.* 10, 100292. <https://doi.org/10.1016/j.gsd.2019.100292>
- 450 Eleftheriadis, K., Ochsenkuhn, K.M., Lymperopoulou, T., Karanasiou, A., Razos, P., Ochsenkuhn-
451 Petropoulou, M., 2014. Influence of local and regional sources on the observed spatial and temporal
452 variability of size resolved atmospheric aerosol mass concentrations and water-soluble species in
453 the Athens metropolitan area. *Atmos. Environ.* 97, 252–261.
454 <https://doi.org/10.1016/j.atmosenv.2014.08.013>
- 455 Gao, J., Tian, H., Cheng, K., Lu, L., Wang, Y., Wu, Y., Zhu, C., Liu, K., Zhou, J., Liu, X., Chen, J., Hao,
456 J., 2014. Seasonal and spatial variation of trace elements in multi-size airborne particulate matters
457 of Beijing, China: Mass concentration, enrichment characteristics, source apportionment, chemical
458 speciation and bioavailability. *Atmos. Environ.* 99, 257–265.
459 <https://doi.org/10.1016/j.atmosenv.2014.08.081>

460 Gao, Y., Lee, S.C., Huang, Y., Chow, J.C., Watson, J.G., 2016. Chemical characterization and source
461 apportionment of size-resolved particles in Hong Kong sub-urban area. *Atmos. Res.* 170, 112–122.
462 <https://doi.org/10.1016/j.atmosres.2015.11.015>

463 Gregory, K., Webster, C., Durk, S., 1996. Estimates of damage to forests in Europe due to emissions of
464 acidifying pollutants. *Energy Policy* 24, 655–664. [https://doi.org/10.1016/0301-4215\(96\)00055-9](https://doi.org/10.1016/0301-4215(96)00055-9)

465 Gujre, N., Mitra, S., Soni, A., Agnihotri, R., Rangan, L., Rene, E.R., Sharma, M.P., 2021. Speciation,
466 contamination, ecological and human health risks assessment of heavy metals in soils dumped with
467 municipal solid wastes. *Chemosphere* 262, 128013.
468 <https://doi.org/10.1016/j.chemosphere.2020.128013>

469 Hakanson, L., 1980. An ecological risk index for aquatic pollution control. a sedimentological approach.
470 *Water Res.* 14, 975–1001. [https://doi.org/10.1016/0043-1354\(80\)90143-8](https://doi.org/10.1016/0043-1354(80)90143-8)

471 Hao, J., Ge, Y., He, S.Y., Lu, N., Wang, Q.G., 2018. Size distribution characteristics of metal elements
472 in air particulate matter during autumn in Nanjing. *Zhongguo Huanjing Kexue/China Environ. Sci.*
473 38, 4409–4414. <https://doi.org/10.19674/j.cnki.issn1000-6923.2018.0493>

474 Huang, X., Olmez, I., Aras, N.K., Gordon, G.E., 1994. Emissions of trace elements from motor vehicles:
475 Potential marker elements and source composition profile. *Atmos. Environ.* 28, 1385–1391.
476 [https://doi.org/10.1016/1352-2310\(94\)90201-1](https://doi.org/10.1016/1352-2310(94)90201-1)

477 Ji, H., Ding, H., Tang, L., Li, C., Gao, Y., Briki, M., 2016. Chemical composition and transportation
478 characteristic of trace metals in suspended particulate matter collected upstream of a metropolitan
479 drinking water source, Beijing. *J. Geochemical Explor.* 169, 123–136.
480 <https://doi.org/10.1016/j.gexplo.2016.07.018>

481 Kampa, M., Castanas, E., 2008. Human health effects of air pollution. *Environ. Pollut.*
482 <https://doi.org/10.1016/j.envpol.2007.06.012>

483 Kandler, K., Schütz, L., Deutscher, C., Ebert, M., Hofmann, H., Jäckel, S., Jaenicke, R., Knippertz, P.,
484 Lieke, K., Massling, A., Petzold, A., Schladitz, A., Weinzierl, B., Wiedensohler, A., Zorn, S.,
485 Weinbruch, S., 2009. Size distribution, mass concentration, chemical and mineralogical
486 composition and derived optical parameters of the boundary layer aerosol at Tinfou, Morocco,
487 during SAMUM 2006. *Tellus, Ser. B Chem. Phys. Meteorol.* 61, 32–50.
488 <https://doi.org/10.1111/j.1600-0889.2008.00385.x>

489 Karaca, F., Anil, I., Alagha, O., 2009. Long-range potential source contributions of episodic aerosol
490 events to PM10 profile of a megacity. *Atmos. Environ.* 43, 5713–5722.
491 <https://doi.org/10.1016/j.atmosenv.2009.08.005>

492 Lee, P.K., Youm, S.J., Jo, H.Y., 2013. Heavy metal concentrations and contamination levels from Asian
493 dust and identification of sources: A case-study. *Chemosphere* 91, 1018–1025.
494 <https://doi.org/10.1016/j.chemosphere.2013.01.074>

495 Li, H., Shi, A., Zhang, X., 2015. Particle size distribution and characteristics of heavy metals in road-
496 deposited sediments from Beijing Olympic Park. *J. Environ. Sci. (China)* 32, 228–237.
497 <https://doi.org/10.1016/j.jes.2014.11.014>

498 Li, X., Wang, L., Wang, Yuesi, Wen, T., Yang, Y., Zhao, Y., Wang, Yingfeng, 2012. Chemical
499 composition and size distribution of airborne particulate matters in Beijing during the 2008
500 Olympics. *Atmos. Environ.* 50, 278–286. <https://doi.org/10.1016/j.atmosenv.2011.12.021>

501 Li, Y., Schwandner, F.M., Sewell, H.J., Zivkovich, A., Tigges, M., Raja, S., Holcomb, S., Molenaar, J.
502 V., Sherman, L., Archuleta, C., Lee, T., Collett, J.L., 2014. Observations of ammonia, nitric acid,
503 and fine particles in a rural gas production region. *Atmos. Environ.* 83, 80–89.

504 <https://doi.org/10.1016/j.atmosenv.2013.10.007>

505 Linak, W.P., Miller, C.A., Wendt, J.O.L., 2000. Comparison of particle size distributions and elemental
506 partitioning from the combustion of pulverized coal and residual fuel oil. *J. Air Waste Manag. Assoc.*
507 50, 1532–1544. <https://doi.org/10.1080/10473289.2000.10464171>

508 Liu, B., Kang, S., Sun, J., Zhang, Y., Xu, R., Wang, Y., Liu, Y., Cong, Z., 2013. Wet precipitation
509 chemistry at a high-altitude site (3,326 m a.s.l.) in the southeastern Tibetan Plateau. *Environ. Sci.*
510 *Pollut. Res.* 20, 5013–5027. <https://doi.org/10.1007/s11356-012-1379-x>

511 Liu, Y., Wang, Q., Zhuang, W., Yuan, Yanli, Yuan, Yani, Jiao, K., Wang, M., Chen, Q., 2018.
512 Calculation of Thallium's toxicity coefficient in the evaluation of potential ecological risk index: A
513 case study. *Chemosphere* 194, 562–569. <https://doi.org/10.1016/j.chemosphere.2017.12.002>

514 Luo, X.S., Xue, Y., Wang, Y.L., Cang, L., Xu, B., Ding, J., 2015. Source identification and
515 apportionment of heavy metals in urban soil profiles. *Chemosphere* 127, 152–157.
516 <https://doi.org/10.1016/j.chemosphere.2015.01.048>

517 Meij, R., te Winkel, H., 2007. The emissions of heavy metals and persistent organic pollutants from
518 modern coal-fired power stations. *Atmos. Environ.* 41, 9262–9272.
519 <https://doi.org/10.1016/j.atmosenv.2007.04.042>

520 Müller, G., 1969. Index of geoaccumulation in sediments of the Rhine River. *Geol. J.* 2, 108–118.

521 Oetari, P.S., Hadi, S.P., Huboyo, H.S., 2019. Trace elements in fine and coarse particles emitted from
522 coal-fired power plants with different air pollution control systems. *J. Environ. Manage.* 250,
523 109497. <https://doi.org/10.1016/j.jenvman.2019.109497>

524 Pacyna, J.M., Pacyna, E.G., 2001. An assessment of global and regional emissions of trace metals to the
525 atmosphere from anthropogenic sources worldwide. *Environ. Rev.* <https://doi.org/10.1139/a01-012>

526 Pan, Y., Tian, S., Li, X., Sun, Y., Li, Y., Wentworth, G.R., Wang, Y., 2015. Trace elements in particulate
527 matter from metropolitan regions of Northern China: Sources, concentrations and size distributions.
528 *Sci. Total Environ.* 537, 9–22. <https://doi.org/10.1016/j.scitotenv.2015.07.060>

529 Pan, Y., Wang, Y., Sun, Y., Tian, S., Cheng, M., 2013. Size-resolved aerosol trace elements at a rural
530 mountainous site in Northern China: Importance of regional transport. *Sci. Total Environ.* 461–462,
531 761–771. <https://doi.org/10.1016/j.scitotenv.2013.04.065>

532 Pan, Y.P., Wang, Y.S., 2015. Atmospheric wet and dry deposition of trace elements at 10 sites in
533 Northern China. *Atmos. Chem. Phys.* 15, 951–972. <https://doi.org/10.5194/acp-15-951-2015>

534 Pancras, J.P., Landis, M.S., Norris, G.A., Vedantham, R., Dvonch, J.T., 2013. Source apportionment of
535 ambient fine particulate matter in Dearborn, Michigan, using hourly resolved PM chemical
536 composition data. *Sci. Total Environ.* 448, 2–13. <https://doi.org/10.1016/j.scitotenv.2012.11.083>

537 Pekney, N.J., Davidson, C.I., 2005. Determination of trace elements in ambient aerosol samples. *Anal.*
538 *Chim. Acta* 540, 269–277. <https://doi.org/10.1016/j.aca.2005.03.065>

539 Polidori, A., Cheung, K.L., Arhami, M., Delfino, R.J., Schauer, J.J., Sioutas, C., 2009. Relationships
540 between size-fractionated indoor and outdoor trace elements at four retirement communities in
541 southern California. *Atmos. Chem. Phys.* 9, 4521–4536. <https://doi.org/10.5194/acp-9-4521-2009>

542 Schwartz, J., Dockery, D.W., Neas, L.M., 1996. Is Daily Mortality Associated Specifically with Fine
543 Particles? *J. Air Waste Manag. Assoc.* 46, 927–939.
544 <https://doi.org/10.1080/10473289.1996.10467528>

545 Shahab, A., Zhang, H., Ullah, H., Rashid, A., Rad, S., Li, J., Xiao, H., 2020. Pollution characteristics and
546 toxicity of potentially toxic elements in road dust of a tourist city, Guilin, China: Ecological and
547 health risk assessment☆. *Environ. Pollut.* 266, 115419.

548 <https://doi.org/10.1016/j.envpol.2020.115419>

549 Shao, P., Tian, H., Sun, Y., Liu, H., Wu, B., Liu, S., Liu, X., Wu, Y., Liang, W., Wang, Y., Gao, J., Xue,
550 Y., Bai, X., Liu, W., Lin, S., Hu, G., 2018. Characterizing remarkable changes of severe haze events
551 and chemical compositions in multi-size airborne particles (PM1, PM2.5 and PM10) from January
552 2013 to 2016–2017 winter in Beijing, China. *Atmos. Environ.* 189, 133–144.
553 <https://doi.org/10.1016/j.atmosenv.2018.06.038>

554 Silva, P.J., Liu, D.Y., Noble, C.A., Prather, K.A., 1999. Size and chemical characterization of individual
555 particles resulting from biomass burning of local Southern California species. *Environ. Sci. Technol.*
556 33, 3068–3076. <https://doi.org/10.1021/es980544p>

557 Tan, J., Zhang, L., Zhou, X., Duan, J., Li, Y., Hu, J., He, K., 2017. Chemical characteristics and source
558 apportionment of PM2.5 in Lanzhou, China. *Sci. Total Environ.* 601–602, 1743–1752.
559 <https://doi.org/10.1016/j.scitotenv.2017.06.050>

560 Taner, S., Pekey, B., Pekey, H., 2013. Fine particulate matter in the indoor air of barbeque restaurants:
561 Elemental compositions, sources and health risks. *Sci. Total Environ.* 454–455, 79–87.
562 <https://doi.org/10.1016/j.scitotenv.2013.03.018>

563 Tian, H., Cheng, K., Wang, Y., Zhao, D., Lu, L., Jia, W., Hao, J., 2012. Temporal and spatial variation
564 characteristics of atmospheric emissions of Cd, Cr, and Pb from coal in China. *Atmos. Environ.* 50,
565 157–163. <https://doi.org/10.1016/j.atmosenv.2011.12.045>

566 Tong, R., Liu, J., Wang, W., Fang, Y., 2020. Health effects of PM2.5 emissions from on-road vehicles
567 during weekdays and weekends in Beijing, China. *Atmos. Environ.* 223, 117258.
568 <https://doi.org/10.1016/j.atmosenv.2019.117258>

569 Wang, F., Chen, D.S., Cheng, S.Y., Li, J.B., Li, M.J., Ren, Z.H., 2010. Identification of regional
570 atmospheric PM10 transport pathways using HYSPLIT, MM5-CMAQ and synoptic pressure
571 pattern analysis. *Environ. Model. Softw.* 25, 927–934.
572 <https://doi.org/10.1016/j.envsoft.2010.02.004>

573 Wang, J., Hu, Z., Chen, Y., Chen, Z., Xu, S., 2013. Contamination characteristics and possible sources
574 of PM10 and PM2.5 in different functional areas of Shanghai, China. *Atmos. Environ.* 68, 221–229.
575 <https://doi.org/10.1016/j.atmosenv.2012.10.070>

576 Wang, J., Zhang, X., Yang, Q., Zhang, K., Zheng, Y., Zhou, G., 2018. Pollution characteristics of
577 atmospheric dustfall and heavy metals in a typical inland heavy industry city in China. *J. Environ.*
578 *Sci. (China)* 71, 283–291. <https://doi.org/10.1016/j.jes.2018.05.031>

579 Wang, Y.S., Yao, L., Wang, L.L., Liu, Z.R., Ji, D.S., Tang, G.Q., Zhang, J.K., Sun, Y., Hu, B., Xin, J.Y.,
580 2014. Mechanism for the formation of the January 2013 heavy haze pollution episode over central
581 and eastern China. *Sci. China Earth Sci.* 57, 14–25. <https://doi.org/10.1007/s11430-013-4773-4>

582 Wei, T., Dong, Z., Kang, S., Zong, C., Rostami, M., Shao, Y., 2019. Atmospheric deposition and
583 contamination of trace elements in snowpacks of mountain glaciers in the northeastern Tibetan
584 Plateau. *Sci. Total Environ.* 689, 754–764. <https://doi.org/10.1016/j.scitotenv.2019.06.455>

585 Wei, X., Gao, B., Wang, P., Zhou, H., Lu, J., 2015. Pollution characteristics and health risk assessment
586 of heavy metals in street dusts from different functional areas in Beijing, China. *Ecotoxicol. Environ.*
587 *Saf.* 112, 186–192. <https://doi.org/10.1016/j.ecoenv.2014.11.005>

588 Williams, J.A., Antoine, J., 2020. Evaluation of the elemental pollution status of Jamaican surface
589 sediments using enrichment factor, geoaccumulation index, ecological risk and potential ecological
590 risk index. *Mar. Pollut. Bull.* 157, 111288. <https://doi.org/10.1016/j.marpolbul.2020.111288>

591 Woszczyk, M., Spsychalski, W., Boluspaeva, L., 2018. Trace metal (Cd, Cu, Pb, Zn) fractionation in

592 urban-industrial soils of Ust-Kamenogorsk (Oskemen), Kazakhstan—implications for the
593 assessment of environmental quality. *Environ. Monit. Assess.* 190, 362.
594 <https://doi.org/10.1007/s10661-018-6733-0>

595 Yu, J.Z., Huang, X.F., 2008. Size distributions of elemental carbon in the atmosphere of a coastal urban
596 area in South China: Characteristics, evolution processes, and implications for the mixing state.
597 *Atmos. Chem. Phys.* 8, 5843–5853. <https://doi.org/10.5194/acp-8-5843-2008>

598 Zereini, F., Alt, F., Messerschmidt, J., Wiseman, C., Feldmann, I., Von Bohlen, A., Müller, J., Liebl, K.,
599 Püttmann, W., 2005. Concentration and distribution of heavy metals in urban airborne particulate
600 matter in Frankfurt am Main, Germany. *Environ. Sci. Technol.* 39, 2983–2989.
601 <https://doi.org/10.1021/es040040t>

602 Zhai, L., Sun, Z., Li, Z., Yin, X., Xiong, Y., Wu, J., Li, E., Kou, X., 2019. Dynamic effects of topography
603 on dust particles in the Beijing region of China. *Atmos. Environ.* 213, 413–423.
604 <https://doi.org/10.1016/j.atmosenv.2019.06.029>

605 Zhang, X., Zhang, K., Lv, W., Liu, B., Aikawa, M., Wang, J., 2019. Characteristics and risk assessments
606 of heavy metals in fine and coarse particles in an industrial area of central China. *Ecotoxicol.*
607 *Environ. Saf.* 179, 1–8. <https://doi.org/10.1016/j.ecoenv.2019.04.024>

608 Zhu, Q., Zhang, X., Dong, S., Gao, L., Liu, G., Zheng, M., 2016. Gas and particle size distributions of
609 polychlorinated naphthalenes in the atmosphere of Beijing, China. *Environ. Pollut.* 212, 128–134.
610 <https://doi.org/10.1016/j.envpol.2016.01.065>

611